The equivalent dynamic stiffness of a visco-elastic half-space in interaction with a periodically supported beam under a moving load

Lu, T.; Metrikine, A.; Steenbergen, M.J.M.M.

DOI
10.1016/j.euromechsol.2020.104065

Publication date
2020

Document Version
Final published version

Published in
European Journal of Mechanics, A/Solids

European Journal of Mechanics / A Solids 84 (2020) 104065

Contents lists available at ScienceDirect

European Journal of Mechanics / A Solids

journal homepage: http://www.elsevier.com/locate/ejmsol

The equivalent dynamic stiffness of a visco-elastic half-space in interaction with a periodically supported beam under a moving load

T. Lu, A.V. Metrikine, M.J.M.M. Steenbergen *

Faculty of Civil Engineering and Geosciences, Delft University of Technology, Stevinweg 1, 2628 CN, Delft, the Netherlands

ARTICLE INFO

Keywords:
Periodically supported beam
Visco-elastic half-space
Moving load
Equivalent stiffness
Quasi-elastic surface wave
Visco-elastic surface wave

ABSTRACT

A periodically supported beam on a visco-elastic half-space is considered to model the vibration of railway tracks. The viscosity of the half-space is assumed to be of the Kelvin-Voigt type. Making use of the concept of equivalent dynamic stiffness, the reaction of the half-space to the sleepers is replaced by a system of identical spring located under each sleeper. The frequency-dependent equivalent stiffness of the springs is a function of the phase shift of vibrations of neighbouring supports. The equivalent stiffness is derived analytically employing the contour integration technique, resulting in a comprehensive expression for different phase velocities of the waves in the beam with respect to the wave speeds of the half-space. Apart from the Rayleigh type surface wave (quasi-elastic wave), an extra visco-elastic surface wave may exist in a visco-elastic half-space depending on the parameters of the half-space and the frequency range. The existence of this second surface wave has not been addressed within the field of train-induced ground vibration. The importance of this wave for the equivalent stiffness is analysed. An effective method to determine the frequency range for the visco-elastic surface wave to exist is proposed.

1. Introduction

With increasing computational power, in recent years numerical methods such as FEM, BEM and hybrid methods are commonly used in modelling train-induced ground vibrations (Hall, 2003; Sheng et al., 2006; Degrande et al., 2006; Yang and Hung, 2009; Galvín et al., 2010; Triepaischajonsak and Thompson, 2015). Analytical methods however retain their significance since they are apt to reveal the underlying mechanisms of the generation of ground vibrations caused by moving trains. Various analytical/semi-analytical models for ground vibration induced by moving trains on open tracks (Sheng et al., 1999; Karlström and Boström, 2006) and in tunnels (Forrest and Hunt, 2006; Metrikine and Vrouwenvelder, 2000; Yuan et al., 2015; Di et al., 2018; Zhou et al., 2020) can be found in the literature. Generally, the analytical/semi-analytical models have high calculation efficiency with reasonable accuracy. A disadvantage however is their assumption of linearity. A comprehensive review can be found in (Lombaert et al., 2015) which covers various prediction methods and mitigation measures for train-induced ground vibration.

The train-induced ground vibration is essentially a three-dimensional problem. Dieterman and Metrikine (1996) introduced the concept of the "equivalent stiffness" to characterize the interaction between the track and an elastic half-space. The track was modelled as an infinitely long Euler-Bernoulli beam whereas the half-space represents the subsoil. The equivalent stiffness was derived analytically for different phase velocities of waves in the beam with respect to the wave speeds in the soil using a contour integration procedure. By replacing the ground reaction by an equivalent foundation with frequency dependent stiffness, the three-dimensional coupled soil-track model was transformed to an equivalent one-dimensional description. Kononov and Wolfert (2000) reconsidered the beam on half-space model in which the viscosity of the half-space is addressed. A different choice of branch cuts, namely the EJP branch cuts (naming after the authors of (Ewing et al., 1957)) was chosen such that a uniform expression for the equivalent stiffness was obtained regardless of the velocity range. In (Metrikine and Popp, 1999), the vibration of a periodically supported beam on an elastic half-space was investigated. This model is a more realistic description of ballasted railway track due to the inclusion of discretely located supports (railpad, sleeper). The expression of the equivalent stiffness of the elastic half-space under each support was derived. It was concluded that the Rayleigh wave velocity is a critical speed besides the ones caused by the periodical nature of the system. Vostroukhov and Metrikine (2003) extended this work to the case of a periodically supported beam on a visco-elastic layer. Utilizing the equivalent 1D model,

* Corresponding author.
E-mail address: M.J.M.M.Steenbergen@tudelft.nl (M.J.M.M. Steenbergen).

https://doi.org/10.1016/j.euromechsol.2020.104065
Received 30 March 2020; Received in revised form 11 June 2020; Accepted 14 June 2020
Available online 3 July 2020

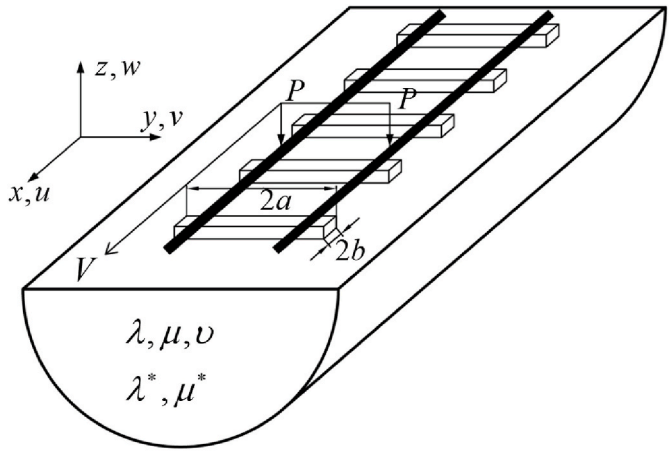

Fig. 1. Periodically supported railway track on a visco-elastic half-space.

the response of the track and the ground can be readily obtained for railway tracks on a half-space (Dieterman and Metrikine, 1997; Chen and Wang, 2006; Steenbergen and Metrikine, 2007) or a layer of soil (Metrikine and Popp, 2000; Vostroukhov and Metrikine, 2003). The equivalent stiffness of a saturated poro-elastic half-space interacting with an infinite beam to a moving load was studied numerically in (Xia et al., 2009). More recently, Sun et al. (2018) investigated the equivalent stiffness for the same case analytically. The steady-state displacements of an Euler-Bernoulli beam resting on a poroelastic half-space subjected to a moving constant load were investigated using the equivalent stiffness in (Shi and Selvadurai, 2016).

In the above-mentioned references in which the concept of the equivalent stiffness is utilized, such stiffness has not been derived for a visco-elastic half-space coupled to a periodically supported beam. The first aim of this paper is to deduce analytically the expression of the equivalent stiffness for this case by means of contour integration. Similar to the approach in (Kononov and Wolfert, 2000), the EJP type of branch cuts (Ewing et al., 1957) is chosen to obtain a uniform expression for the entire velocity range. As an additional novelty, it is established that an extra visco-elastic surface wave may exist in a visco-elastic half-space besides the Rayleigh type surface wave as described in the literature (Currie et al., 1977; Currie and O'Leary, 1978; Carcione, 1992; Romeo, 2001). For typical properties of underlying subsoil of railways, it is found that the second surface wave may exist in a certain frequency range. The contribution of this wave to the equivalent stiffness and consequently the dynamic response of the system cannot be ignored. This issue has not been addressed in the literature dedicated to railway-induced ground vibration. This work proposes also an effective method to determine the frequency range for the visco-elastic wave to exist.

The paper is structured as follows. Section 2 presents the model and derivation of the equivalent stiffness of a visco-elastic half-space in interaction with a periodically supported beam. In Section 3 the equivalent stiffness is evaluated analytically making use of the contour integration. The results are validated by comparison with direct numerical integration as well as the corresponding elastic half-space case. The importance of the second surface wave is addressed explicitly in Section 4. In Section 5, the frequency range in which the second surface wave exists is analysed. An effective way to determine the frequency range is proposed regardless of the system parameters. The influences of both viscosity and Poisson's ratio on this frequency range are analysed. Section 6 summarises the conclusions of this paper.

2. Model and equivalent stiffness

Fig. 1 shows the model adopted to study the steady-state vibrations of a railway track. Two infinitely long Euler-Bernoulli beams (rails) are supported by equi-distantly distributed supports (sleepers) resting on a half-space (subsoil) consisting of a homogeneous, isotropic visco-elastic material. This work adopts the Kelvin-Voigt model to describe soil behaviour. Although other models such as the hysteretic damping model (Verruijt and Cordova, 2001) may be more appropriate in this context, the description is chosen in line with previous work on the equivalent dynamic stiffness (Metrikine and Popp, 2000; Kononov and Wolfert, 2000; Vostroukhov and Metrikine, 2003; Steenbergen and Metrikine, 2007), allowing for a direct comparison. The method itself however allows for a similar study on the basis of other constitutive damping models. For the system parameters, ν is the Poisson's ratio and ρ is the density of the half-space. λ and μ are the Lamé constants. Each support consists of a rigid sleeper and a railpad which is modelled as a spring-dashpot element. Each sleeper occupies a rectangular contact area $2a \times 2b$ as shown in Fig. 1. The distance between the centerlines of two neighbouring sleepers is denoted as d. A harmonic load $P(t) = P_0 \exp(\mathrm{i}\Omega t)$ ($\mathrm{i} = \sqrt{-1}$) moves uniformly at a speed V on the track. Considering the symmetry of the loading with respect to the centerline $y = 0$ of the track, only one equation of motion for one beam is presented. The coordinate system is shown in Fig. 1 as well.

The governing equations of motion of the coupled system can be written as follows.

The equation of motion for a visco-elastic half-space takes the form:

$$\widehat{\mu}\Delta\mathbf{u} + (\widehat{\lambda} + \widehat{\mu})\nabla(\nabla \cdot \mathbf{u}) = \rho\partial_{tt}\mathbf{u} \tag{1}$$

where $\mathbf{u}(x, y, z, t) = [u(x, y, z, t), v(x, y, z, t), w(x, y, z, t)]^T$ is the displacement vector. To account for the viscosity according to the Voigt phenomenological model, the Lamé constants λ and μ of the elastic case are replaced by $\widehat{\lambda} = \lambda + \lambda^*\partial/\partial t$ and $\widehat{\mu} = \mu + \mu^*\partial/\partial t$ in the governing equation (1) of the soil, respectively.

To solve Eq. (1), the Helmholtz decomposition can be used. However, based on the assumption of zero shear stress at the soil-sleeper interface that is adopted in this paper, two so-called stress functions

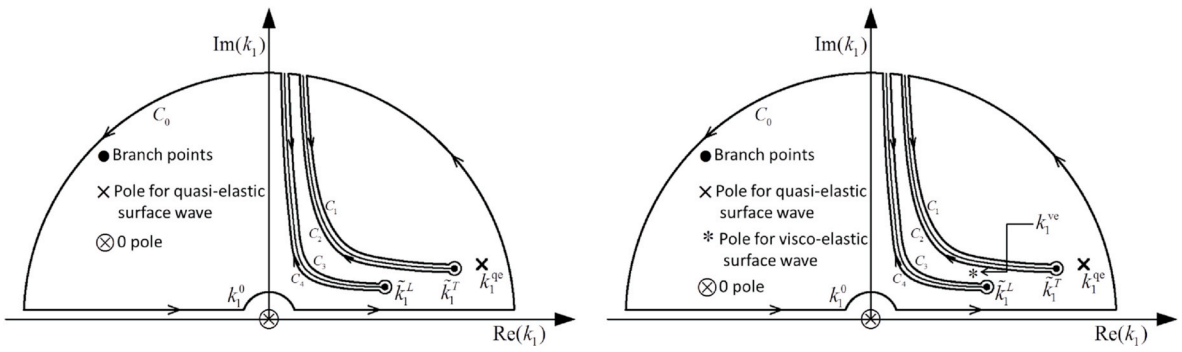

Fig. 2. The contour of integration and singular points of Eq. (16): (a) one pole, (b) two poles.

$\phi(x,y,z,t)$ and $\psi(x,y,z,t)$ can be employed to decouple the original three-dimensional wave equations as shown in (Lamb, 1904; Dieterman and Metrikine, 1996; Vostroukhov, 2002). Hence, the governing equations for the visco-elastic half-space become:

$$\left(c_{\mathrm{L}}^2+\delta_{\mathrm{L}}\frac{\partial}{\partial t}\right)\triangle\phi=\frac{\partial^2\phi}{\partial t^2};\quad \left(c_{\mathrm{T}}^2+\delta_{\mathrm{T}}\frac{\partial}{\partial t}\right)\triangle\psi=\frac{\partial^2\psi}{\partial t^2}\psi \tag{2}$$

where $c\mathrm{L}=\sqrt{(\lambda+2\mu)/\rho}$ is the speed of the compressional wave (P-wave) and $c\mathrm{T}=\sqrt{\mu/\rho}$ the speed of the shear wave (S-wave). The viscous constants in Eq. (2) are defined as $\delta_{\mathrm{T}}=\mu^*/\rho, \delta_{\mathrm{L}}=(\lambda^*+2\mu^*)/\rho$. The displacements of the half-space are expressed in terms of the stress functions as (Lamb, 1904; Dieterman and Metrikine, 1996; Vostroukhov, 2002):

$$u=\frac{\partial\phi}{\partial x}+\frac{\partial^2\psi}{\partial x\partial z},\ v=\frac{\partial\phi}{\partial y}+\frac{\partial^2\psi}{\partial y\partial z},\ w=\left(\frac{\partial\phi}{\partial z}+\frac{\partial^2\psi}{\partial z^2}\right)-\frac{\rho}{\tilde{\mu}}\frac{\partial^2\psi}{\partial t^2}. \tag{3}$$

The equation that governs the vertical motion of the beam is (Metrikine and Popp, 1999):

$$mW^0_{,tt}+EIW^0_{,xxxx}=-P_0\exp(i\Omega t)\delta(x-Vt)-K\times\sum_{n=-\infty}^{\infty}\left(W^0(x,t)-W_{\mathrm{s}}^n(t)\right)\delta(x-nd) \tag{4}$$

where m is the density of the beam, EI is the bending stiffness. K is the stiffness of the railpad, W^0 and W_{s}^n are the vertical displacements of the beam and the nth sleeper, respectively.

A uniform stress distribution is assumed at the interface $z=0$ of the half-space (Metrikine and Popp, 1999):

$$\sigma_{zz}=\frac{1}{4ab}\sum_{n=-\infty}^{\infty}\left\{K\left(W^0(nd,t)-W_{\mathrm{s}}^n(\mathrm{t})\right)-M\frac{\partial^2}{\partial t^2}W_{\mathrm{s}}^n(t)\right\}H(a-|y|)H(b-|x-nd|), \tag{5}$$

$$\tau_{xz}(x,y,0,t)=\tau_{yz}(x,y,0,t)=0 \tag{6}$$

in which M is the sleeper mass and H is the Heaviside step function.

Displacement compatibility along the centre-line $y=0$ is assumed between the sleepers and the half-space for the vertical motion at the interface $z=0$ (Metrikine and Popp, 1999):

$$W_{\mathrm{s}}^n(t)=W(nd,0,0,t). \tag{7}$$

Eqs. (2)–(7) complete the mathematical description of the problem.

The technique of integral transformation is used to transform the problem statement to wave-number and frequency domain. The following integral Fourier transforms are adopted:

$$\{f,g\}(k_1,k_2,z,\omega)=\int_{-\infty}^{\infty}\int_{-\infty}^{\infty}\int_{-\infty}^{\infty}\{\phi,\psi\}(x,y,z,t)\exp(\mathrm{i}\omega\mathrm{t}-\mathrm{i}(\mathrm{k}_1\mathrm{x}+\mathrm{k}_2\mathrm{y}))\mathrm{d}t\mathrm{d}x\mathrm{d}y$$

$$\mathrm{W}^0_{\omega,\mathrm{k}_1}(\mathrm{k}_1,\omega)=\int_{-\infty}^{\infty}\int_{-\infty}^{\infty}\mathrm{W}^0(\mathrm{x},\mathrm{t})\exp(\mathrm{i}\omega\mathrm{t}-\mathrm{i}\mathrm{k}_1\mathrm{x})\mathrm{d}t\mathrm{d}x. \tag{8}$$

All the governing equations, boundary and interface conditions Eqs. (2)–(7) are then transformed to the frequency and wave-number domain using Eq. (8). One is referred to (Metrikine and Popp, 1999) for the detailed derivation of the expression of the equivalent stiffness since the same procedure is used here. It is worth mentioning that the general solutions of Eq. (2) after applying the Fourier transforms (Eq. (8)) are assumed to be:

$$f=A(k_1,k_2,\omega)\exp(-z\tilde{R}_{\mathrm{L}}),\ g=B(k_1,k_2,\omega)\exp(-z\tilde{R}_{\mathrm{T}}) \tag{9}$$

Accounting for the proper behaviour for large positive values of z. In Eq. (9)

$$\tilde{R}_{\mathrm{L,T}}=\sqrt{k_1^2+k_2^2-\omega^2/\tilde{c}_{\mathrm{L,T}}^2},\ \mathrm{Re}(\tilde{\mathrm{R}}_{\mathrm{L,T}})>0 \tag{10}$$

where

$$\tilde{c}_{\mathrm{L,T}}^2=c_{\mathrm{L,T}}^2\left(1-\mathrm{i}\omega\delta_{\mathrm{L,T}}\Big/\mathrm{c}_{\mathrm{L,T}}^2\right). \tag{11}$$

The expression of the equivalent stiffness from the half-space to the support can be written as (Metrikine and Popp, 1999):

$$\chi_{\mathrm{h-s,s}}=\left(\frac{\omega^2}{4\pi^2\tilde{\mu}\tilde{c}_{\mathrm{T}}^2}\sum_{n=-\infty}^{\infty}\int_{-\infty}^{\infty}\int_{-\infty}^{\infty}\frac{\tilde{R}_L}{\Delta}\frac{\sin(bk_1)}{bk_1}\frac{\sin(ak_2)}{ak_2}\exp(i(k_1d-q(\omega))n)\mathrm{d}k_1\mathrm{d}k_2\right)^{-1} \tag{12}$$

where

$$\Delta=\left(2\left(k_1^2+k_2^2\right)-\omega^2/\tilde{c}_{\mathrm{T}}^2\right)^2-4\tilde{R}_{\mathrm{L}}\tilde{R}_{\mathrm{T}}\left(k_1^2+k_2^2\right). \tag{13}$$

In Eq. (12), $\tilde{\mu}=\mu-\mathrm{i}\omega\mu^*$ and $q(\omega)$ is the phase shift of the vibrations of two neighbouring supports and is given by (Metrikine and Popp, 1999; Vostroukhov and Metrikine, 2003):

$$q(\omega)=\frac{(\omega+\Omega)d}{V}. \tag{14}$$

Hence, the equivalent stiffness (Eq. (12)) of the springs under supports is established. Note that Eq. (12) is the same as Eq. (20) in (Metrikine and Popp, 1999), however, including the viscosity by replacing c_{T}^2 and μ of Eq. (20) in (Metrikine and Popp, 1999) with $\tilde{c}_{\mathrm{T}}^2$ and $\tilde{\mu}$, respectively.

3. Evaluation of the equivalent stiffness

To evaluate the equivalent stiffness, the denominator of Eq. (12) must be computed. This denominator can be rewritten as

$$I_{\mathrm{h-s,s}}=\frac{1}{2iab}\frac{\omega^2}{4\pi^2\tilde{\mu}\tilde{c}_{\mathrm{T}}^2}\sum_{n=-\infty}^{\infty}\int_{-\infty}^{\infty}\int_{-\infty}^{\infty}\left(\frac{\tilde{R}_{\mathrm{L}}\sin(ak_2)}{k_1k_2\Delta}(\exp(ik_1b)-\exp(-ik_1b))\exp(i(k_1d-q(\omega))n)\right)\mathrm{d}k_1\mathrm{d}k_2 \tag{15}$$

The following auxiliary integral with respect to k_1 is introduced (Metrikine and Popp, 1999):

$$Z(r)=\int_{-\infty}^{\infty}\frac{\tilde{R}_{\mathrm{L}}}{\Delta}\frac{\exp(ik_1r)}{k_1}\mathrm{d}k_1=\int_{-\infty}^{\infty}\frac{\tilde{R}_{\mathrm{L}}}{\Delta}\frac{(\exp(ik_1r)-1)}{k_1}\mathrm{d}k_1 \tag{16}$$

where r is a real value. The introduction of "1" in the numerator accounts for the contribution of the pole $k_1^0=0$. It does not influence the result of integration since $\int_{-\infty}^{+\infty}\{\tilde{R}_{\mathrm{L}}/(k_1\Delta)\}\mathrm{d}k_1=0$ (Metrikine and Popp, 1999).

Using the auxiliary integral, Eq. (15) can be written as

$$I_{\mathrm{h-s,s}}=\frac{1}{2iab}\frac{\omega^2}{4\pi^2\tilde{\mu}\tilde{c}_{\mathrm{T}}^2}\int_{-\infty}^{\infty}\left(\frac{\sin(ak_2)}{k_2}\sum_{n=-\infty}^{\infty}\exp(-iq(\omega)n)(Z(nd+b)-Z(nd-b))\right)\mathrm{d}k_2. \tag{17}$$

Denoting the summation in the integrand of Eq. (17) as S and evaluating yields:

$$\begin{aligned}S&=\sum_{n=-\infty}^{\infty}\exp(-iq(\omega)n)(Z(nd+b)-Z(nd-b))=\\&Z(b)-Z(-b)+\sum_{1}^{\infty}\{\exp(-iq(\omega)n)(Z(nd+b)-Z(nd-b))+\exp(iq(\omega)n)(Z(b-nd)-Z(-nd-b))\}\\&=2Z(b)+\sum_{1}^{\infty}\{(\exp(iq(\omega)n)+\exp(-iq(\omega)n))(Z(nd+b)-Z(nd-b))\},\end{aligned} \tag{18}$$

where the terms $Z(b), Z(nd+b), Z(nd-b)$ can be evaluated after obtaining an analytical expression for the auxiliary integral Eq. (16).

3.1. Branch points and branch cuts

Eq. (16) is evaluated using contour integration. The EJP branch cuts (Ewing et al., 1957) are used here. Firstly, the branch points are specified from the radicals $\tilde{R}_{\mathrm{L,T}}(k_1^{\mathrm{L,T}})=0$, resulting in

$$\tilde{k}_1^{\mathrm{L}}=\pm\sqrt{\omega^2/\tilde{c}_{\mathrm{L}}^2}-k_2^2=\pm(\tilde{\alpha}_{\mathrm{L}}+\mathrm{i}\tilde{t}_{\mathrm{L}}),\tilde{k}_1^{\mathrm{T}}=\pm\sqrt{\omega^2/\tilde{c}_{\mathrm{T}}^2}-k_2^2=\pm(\tilde{\alpha}_{\mathrm{T}}+\mathrm{i}\tilde{t}_{\mathrm{T}}). \tag{19}$$

It is assumed that $k_1>0$. The branch cuts can be chosen such that $\mathrm{Re}(\tilde{\mathrm{R}}_{\mathrm{L,T}})>0$ everywhere on the path of integration in accordance with the assumed solution in Eq. (9). To meet these conditions, the cuts should satisfy the following equations:

$$\mathrm{Re}(\tilde{\mathrm{R}}_{\mathrm{L,T}})=0\Leftrightarrow\mathrm{Im}(\gamma(\mathrm{k}_1))=0\wedge\mathrm{Re}(\gamma(\mathrm{k}_1))<0 \tag{20}$$

where

$$\gamma(k_1)=k_1^2+k_2^2-\omega^2\Big/\tilde{c}_{\mathrm{L,T}}^2. \tag{21}$$

The branch cuts are governed by the parametric equations:

$$k_1^{\mathrm{L,T}}=\alpha_{\mathrm{L,T}}+\mathrm{i}t_{\mathrm{L,T}}. \tag{22}$$

Substituting $k_1^{L,T}$ into Eq. (20), one obtains

$$\alpha_{\mathrm{L,T}}=\frac{\omega^3\delta_{\mathrm{L,T}}}{2(c_{\mathrm{L}}^4+\omega^2\delta_{\mathrm{L,T}}^2)t_{\mathrm{L,T}}}. \tag{23}$$

Note that $\tilde{\alpha}_{\mathrm{L,T}}$ and $\tilde{t}_{\mathrm{L,T}}$ in Eq. (19) are functions of k_2 and ω. The same holds for $\alpha_{\mathrm{L,T}}$ and $t_{\mathrm{L,T}}$ in Eq. (22).

3.2. Poles

For a homogeneous, isotropic elastic half-space, it is well-known that in this case there is one and only one root of the secular equation $\Delta=0$ (Achenbach, 1975). This means the integrand of Eq. (15) has only one pole which represents the Rayleigh surface wave. However, in a half-space made of homogeneous, isotropic, linearly viscoelastic material, more than one surface wave may exist. It is found that two roots (representing two surface waves) of the secular equation (13) which satisfy the traction-free boundary condition and radiation condition may exist, depending on the material properties and the frequency (Currie et al., 1977; Currie and O'Leary, 1978). Fig. 2(a) shows an integration contour with only the Rayleigh type pole. For the parameters used in Fig. 2(b), two poles, related to two surface waves exist. The surface wave whose characteristics are close to the classical Rayleigh wave of the corresponding elastic body is termed as the "quasi-elastic wave" (pole k_1^{qe} in Fig. 2(b)), whereas the other surface wave is called a visco-elastic surface wave (pole k_1^{ve} in Fig. 2(b)) in (Currie et al., 1977; Currie and O'Leary, 1978). The complete contour integration in Fig. 2(b) must include the contributions of both poles k_1^{qe} and k_1^{ve}.

3.3. Analytical expression of the equivalent stiffness

The branch cuts, branch points, poles and integration contours are shown in Fig. 2. Since the contributions of integration along the big semicircular contour C_0 and along the circular contours around the branch points are zero (Kononov and Wolfert, 2000), Eq. (16) can be solved as

$$Z(r)=2\pi\mathrm{i}\sum_{1}^{\mathrm{N}}\left(\frac{\tilde{R}_{\mathrm{L}}}{\Delta}\frac{(\exp(ik_1r)-1)}{k_1}\right)_{k_1=k_{pN}}-\int_{C_1+C_2+C_3+C_4} \tag{24}$$

according to the residue theorem, where k_{pN} are the poles derived from Eq. (13).

Substituting Eq. (24) into Eq. (18), the summation in Eq. (18) can be elaborated in the same manner as shown in (Metrikine and Popp, 1999). The contribution of the poles can be written as:

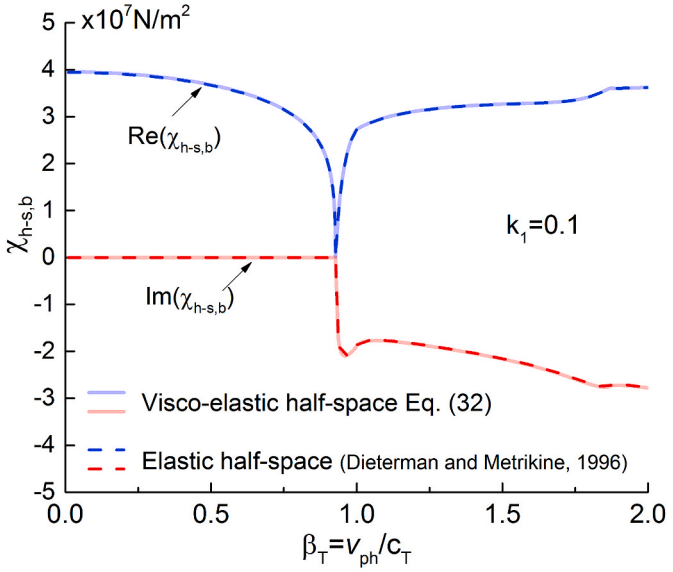

Fig. 3. Equivalent stiffness of a beam directly on a half-space.

$$S_p = 4\pi i\left(\frac{\tilde{R}_L}{\mathrm{d}\Delta/\mathrm{d}k_1}\frac{\exp(ik_1 b)-1}{k_1}\right)_{k_1=k_1^{qe}} + 2\pi i\left(\frac{\tilde{R}_L}{\mathrm{d}\Delta/\mathrm{d}k_1}\frac{Q}{k_1}\right)_{k_1=k_1^{qe}} \tag{25}$$

if only the quasi-elastic wave exists as illustrated in Fig. 2(a), or

$$\begin{aligned} S_p = {} & 4\pi i\left(\frac{\tilde{R}_L}{\mathrm{d}\Delta/\mathrm{d}k_1}\frac{\exp(ik_1 b)-1}{k_1}\right)_{k_1=k_1^{qe}} + 2\pi i\left(\frac{\tilde{R}_L}{\mathrm{d}\Delta/\mathrm{d}k_1}\frac{Q}{k_1}\right)_{k_1=k_1^{qe}} \\ & + 4\pi i\left(\frac{\tilde{R}_L}{\mathrm{d}\Delta/\mathrm{d}k_1}\frac{\exp(ik_1 b)-1}{k_1}\right)_{k_1=k_1^{ve}} + 2\pi i\left(\frac{\tilde{R}_L}{\mathrm{d}\Delta/\mathrm{d}k_1}\frac{Q}{k_1}\right)_{k_1=k_1^{ve}}. \end{aligned} \tag{26}$$

where

$$Q = \frac{2i\sin(k_1 b)(\cos(q)-\exp(ik_1 d))}{\cos(k_1 d)-\cos(q)}. \tag{27}$$

The contribution of branch cuts can be written as follows, taking C_1 as an example:

$$\begin{aligned} S_{C_1} &= 2\int_{\infty}^{\tilde{t}_T}\left(\frac{\tilde{R}_L}{\Delta}\frac{\exp(ik_1 b)-1}{k_1}\right)\mathrm{d}k_1^T + \int_{\infty}^{\tilde{t}_T}\left(\frac{\tilde{R}_L}{\Delta}\frac{Q}{k_1}\right)\mathrm{d}k_1^T \\ &= -2\int_{\tilde{t}_T}^{\infty}\left(\frac{\tilde{R}_L}{\Delta}\frac{\exp(ik_1 b)-1}{k_1}\right)\mathrm{d}k_1^T - \int_{\tilde{t}_T}^{\infty}\left(\frac{\tilde{R}_L}{\Delta}\frac{Q}{k_1}\right)\mathrm{d}k_1^T \end{aligned} \tag{28}$$

where k_1^T is given by Eq. (22) and $\tilde{t}_T$ is given in Eq. (19). S_{C_2} through S_{C_4} can be obtained in a similar way. Thus

$$S = S_p - (S_{C_1} + S_{C_2} + S_{C_3} + S_{C_4}) \tag{29}$$

and

$$I_{h-s,s} = \frac{1}{2iab}\frac{\omega^2}{4\pi^2\tilde{\mu}\tilde{c}_T^2}\int_{-\infty}^{\infty}\left(\frac{\sin(ak_2)}{k_2}S\right)\mathrm{d}k_2. \tag{30}$$

The equivalent stiffness is the reciprocal of Eq. (30), namely

$$\chi_{h-s,s}(\omega) = (I_{h-s,s})^{-1} = \left(\frac{1}{2iab}\frac{\omega^2}{4\pi^2\tilde{\mu}\tilde{c}_T^2}\int_{-\infty}^{\infty}\left(\frac{\sin(ak_2)}{k_2}S\right)\mathrm{d}k_2\right)^{-1}. \tag{31}$$

Eq. (12) can be reduced to the case of a beam on a visco-elastic half-space which was investigated in (Kononov and Wolfert, 2000); in this case the equivalent stiffness becomes

$$\chi_{h-s,b}(k_1,\omega) = \left(\frac{-\omega^2}{2\pi\tilde{\mu}\tilde{c}_T^2}\int_{-\infty}^{\infty}\frac{\tilde{R}_L}{\Delta}\frac{\sin(a_{beam}k_2)}{a_{beam}k_2}\mathrm{d}k_2\right)^{-1}. \tag{32}$$

In Eq. (32) a_{beam} is the width of the beam on the half-space. The above equation can be evaluated using the same contour integration technique presented to evaluate Eq. (12) previously. Eq. (32) is the same as obtained in (Kononov and Wolfert, 2000). However, the contribution of the possible extra pole (the visco-elastic surface wave) is not discussed in (Kononov and Wolfert, 2000).

4. Verification of the solution and the contribution of the visco-elastic surface wave

In this section, the derived expression is verified by comparison with both the analytical expression for the elastic half-space case and the results from direct numerical integration of the latter. The importance of the contribution of the visco-elastic wave is addressed. The following soil parameters are adopted from (Vostroukhov and Metrikine, 2003):

$$\mu = 2.6\times10^7\,\mathrm{N/m^2},\ \rho = 1960\,\mathrm{kg/m^3},\ \nu = 0.3 \tag{33}$$

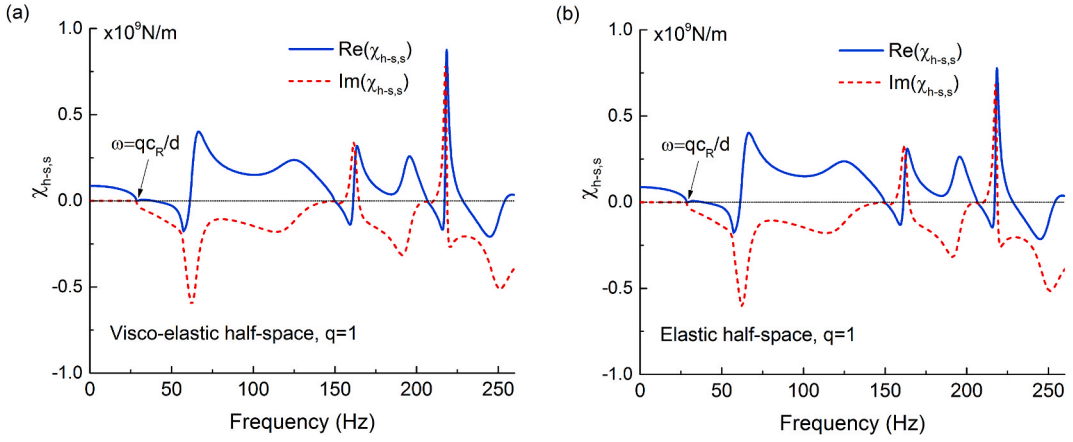

Fig. 4. (a) Equivalent stiffness of a visco-elastic half-space to periodically supported beam with small viscosity using Eq. (31), (b) Equivalent stiffness of an elastic half-space to periodically supported beam according to (Metrikine and Popp, 1999).

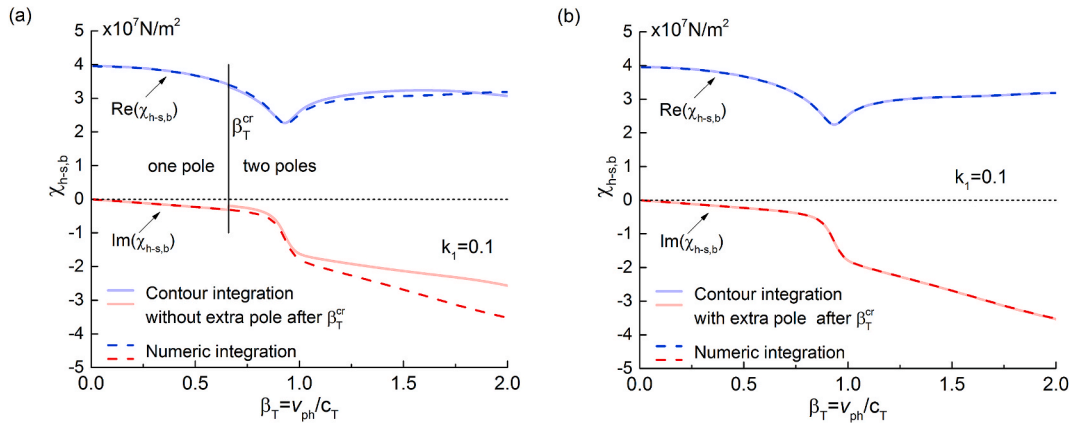

Fig. 5. Comparison of equivalent stiffness obtained using contour integration and numerical integration for a beam directly on a visco-elastic half-space for $\kappa = 1\times 10^{-2}$ s: (a) Contour integration without the extra pole, (b) Contour integration with the extra pole after $\beta_T > \beta_T^{cr}$.

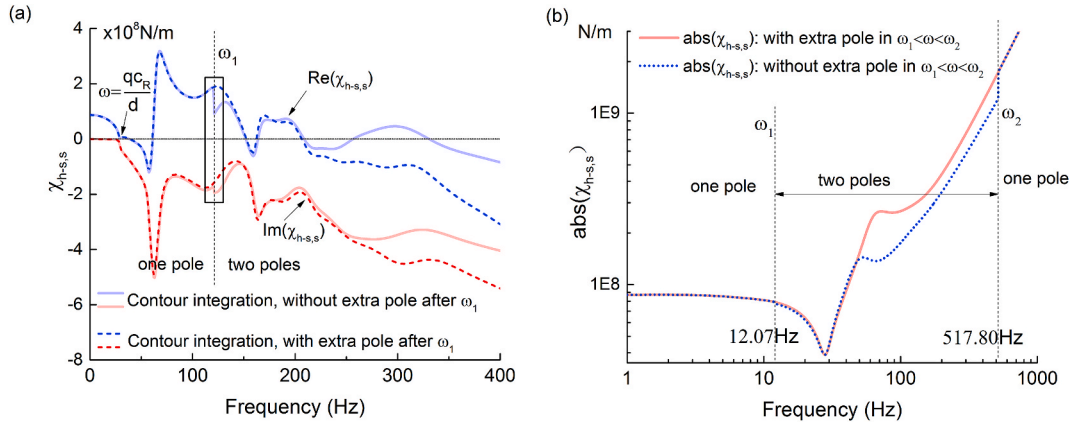

Fig. 6. Equivalent stiffness of a periodically supported beam on visco-elastic half-space: (a) $\kappa = 1 \times 10^{-4}$ s, (b) $\kappa = 1 \times 10^{-3}$ s.

Table 1
The first critical frequency ω_1 versus damping ratio.

κ	k_2			
	0.1	5	10	30
1×10^{-5} s	1206.88 Hz	1206.88 Hz	1206.88 Hz	1206.88 Hz
1×10^{-4} s	120.69 Hz	120.69 Hz	120.69 Hz	120.69 Hz
5×10^{-4} s	24.14 Hz	24.14 Hz	24.14 Hz	24.14 Hz
1×10^{-3} s	12.07 Hz	12.07 Hz	12.07 Hz	12.07 Hz

for the numerical evaluations. For simplicity, $\mu^*/\mu = \lambda^*/\lambda = \kappa$ is assumed hereafter. However, the above-obtained expressions for $\chi_{\mathrm{h-s,s}}$ and $\chi_{\mathrm{h-s,b}}$ are also valid for the case $\mu^*/\mu \neq \lambda^*/\lambda$.

4.1. Half-space with relatively small viscosity

To show the validity of the expressions obtained in this paper for a visco-elastic half-space, the results are compared to those of the elastic half-space case. Firstly, the case of a half-space interacting directly (without the supports) with a beam is considered. The width of the beam is assumed to be 3.2 m, namely $a_{\mathrm{beam}} = 3.2$ in Eq. (32). In Fig. 3 the result computed from Eq. (32) with a small viscosity ($\kappa = 1\times 10^{-7}$ s) is compared to that from (Dieterman and Metrikine, 1996) for an elastic half-space. The parameter v_{ph} is the phase velocity in x direction and is defined as $v_{\mathrm{ph}} = \omega/\mathrm{k_1}$. It can be seen that the results agree with each other perfectly.

In Fig. 4 the case of a periodically supported beam (Fig. 1) is considered. The soil parameters are according to Eq. (33) whereas the geometry of the sleepers is defined according to (Vostroukhov and Metrikine, 2003):

$$2a = 2.7\mathrm{m},\ \mathrm{d} = 0.6\mathrm{m},\ 2\mathrm{b} = 0.27\mathrm{m}. \tag{34}$$

In Fig. 4(a) the equivalent stiffness of a visco-elastic half-space for a constant phase shift $q = 1.0$ is calculated considering a small viscosity ($\kappa = 1\times 10^{-7}$ s) using Eq. (31). For frequencies smaller than $\omega = qc_{\mathrm{R}}/\mathrm{d}$, the imaginary part of the equivalent stiffness is zero because no waves are generated (Metrikine and Popp, 1999). At the frequencies where the equivalent stiffness equals to zero, the frequency satisfies $\omega d/c_{\mathrm{R}} = |q(\omega) + 2\pi n|$ where n is an integer (Metrikine and Popp, 1999). The result is compared with Fig. 4(b) in which the equivalent stiffness of an elastic half-space is evaluated based on the expression obtained in (Metrikine and Popp, 1999) using the same parameters of the soil and sleepers. Once again there is a perfect match between the slightly viscous half-space and the elastic half-space cases. The comparisons in Figs. 3 and 4 conform the validity of expressions obtained in this work for the equivalent stiffness.

4.2. Half-space with relatively large viscosity

When a relatively large viscosity is considered for the half-space, an extra root of the secular equation $\Delta = 0$ may appear for certain parameters, meaning an extra pole of Eq. (15). Physically this implies the existence of an extra visco-elastic surface wave in the half-space caused by the viscosity. Some discussions on the existence of an extra wave can

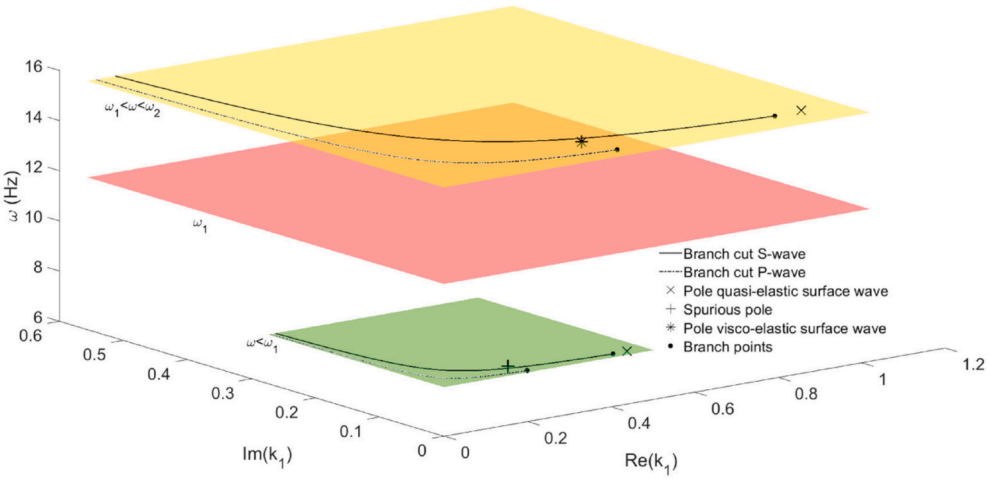

Fig. 7. Transition of the number of poles around ω_1 for $\kappa = 1 \times 10^{-3}$ s.

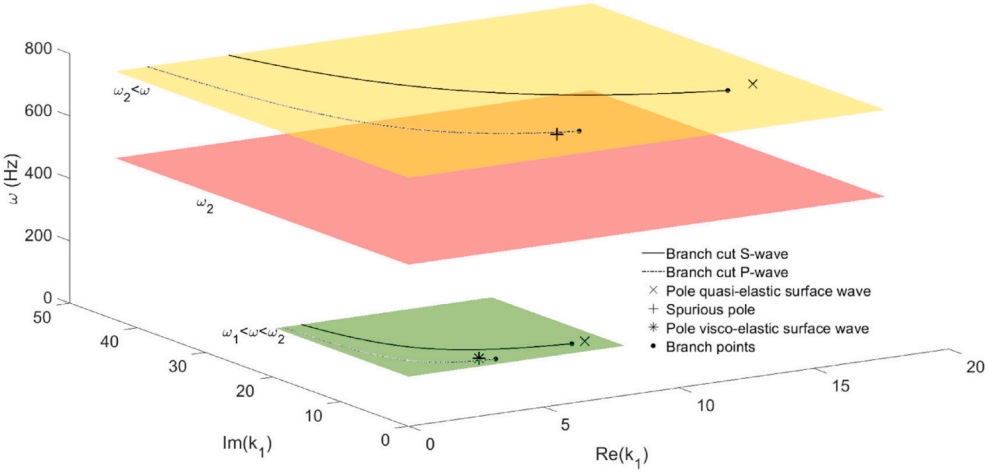

Fig. 8. Transition of the number of poles around ω_2 for $\kappa = 1 \times 10^{-3}$ s.

be found in (Currie et al., 1977; Currie and O'Leary, 1978; Carcione, 1992; Romeo, 2001; Chiriţă et al., 2014; Sharma, 2019). In this subsection the contribution of this second wave to the equivalent stiffness is analysed.

4.2.1. *Beam on a visco-elastic half-space*

In Fig. 5(a) the equivalent stiffness obtained from contour integration with only the quasi-elastic wave (the conventional Rayleigh type) considered is compared to that obtained from direct numerical integration for relatively large viscosity. It is found that at a certain value of β_T^{cr}, a discontinuity of the stiffness occurs. This discontinuity indicates that a visco-elastic wave appears after β_T^{cr}. Using Cauchy's argument principle (Ying and Katz, 1988), two roots (equivalently two poles of the integrand in Eq. (32)) can be obtained from the secular equation (13) for $\beta_T > \beta_T^{cr}$. Results from contour integration with both poles included for $\beta_T > \beta_T^{cr}$ and from direct numerical integration of the expression are shown to match completely in Fig. 5(b).

4.2.2. *Periodically supported beam on a visco-elastic half-space*

In Fig. 6(a), the equivalent stiffness of a visco-elastic half-space to a periodically supported beam is computed with and without the extra pole which appears after a critical frequency ω_1, for damping ratio $\kappa = 1 \times 10^{-4}$ s. Similar to the case of a continuous beam on a half-space shown in Fig. 5, the omission of the extra wave leads to discontinuity of the equivalent stiffness and erroneous results after the critical frequency ω_1. However, when damping is increased, there may be an upper limit-frequency for two poles as shown in Fig. 6(b). In Fig. 6(b), the absolute values of the equivalent stiffnesses are shown using a logarithmic scale for $\kappa = 1 \times 10^{-3}$ s. Two waves can be observed to exist in the frequency range $\omega_1 < \omega < \omega_2$.

Figs. 5 and 6 demonstrate the importance of taking into account the extra visco-elastic wave for the evaluation of the equivalent stiffness and eventually the prediction of the dynamic response to a stationary/moving load. The contribution of this second surface wave can be relatively significant with respect to the first type as found in (O'Leary, 1988; O'Leary, 1989) where the forced vibration of a semi-infinite viscoelastic medium due to an oscillating load applied at the free surface is investigated.

4.3. *Advantages of the proposed analytical method*

The proposed analytical method provides an exact expression for evaluating the equivalent stiffness. It has been shown in Fig. (5) that the prediction on the basis of the analytical method matches that from numerical integration for a beam on half-space. The agreement of the results confirms the correctness of the contour integration procedure presented in this paper. For the case of a periodically supported beam on a visco-elastic half-space, direct numerical integration requires a truncation of the number of supports. A relatively large number of sleepers is required to obtain a convergent result. Furthermore, the number of

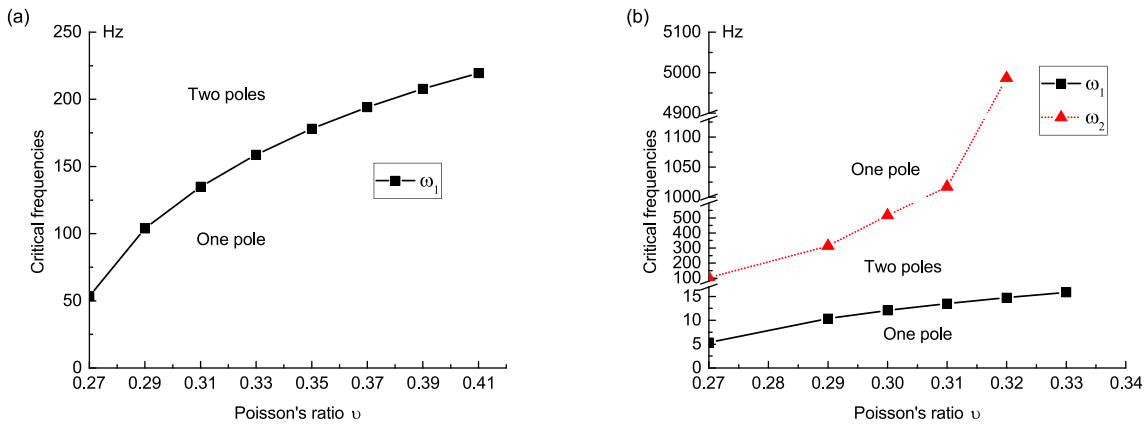

Fig. 9. The critical frequencies versus Poisson's ratio: (a) $\kappa = 1 \times 10^{-4}$ s, (b) $\kappa = 1 \times 10^{-3}$ s.

supports needed is different for different frequencies. In summary, on one hand, the proposed analytical method gives an exact solution without any truncation. On the other hand, it is far more computationally efficient than the direct numerical integration.

5. The frequency range for two surface waves to exist in a visco-elastic half-space

In (Currie et al., 1977; Carcione, 1992) it is stated that the second surface wave exists for certain values of the material parameters as well as a given range of frequencies. In this section a way is presented to determine such frequency range for two waves to exist for specific parameters. Before proceeding, one important observation can be made from Fig. 6. To obtain the equivalent stiffness from Eq. (12), integration of k_2 should be carried out. The poles shown in Fig. 2 depend on both k_2 and the frequency ω. For different k_2, the poles are different. One may expect that for different k_2, a different critical frequency may exist which corresponds to appearance of the second surface wave. However, from Fig. 6 it is shown that there is one discontinuity, thus one critical frequency for all the k_2. To examine the dependence of the critical frequency on the wavenumber k_2, the critical frequency ω_1 is calculated for various damping values and k_2 shown in Table 1. Since the convergence over k_2 is relatively fast, the calculation is only performed till $k_2 = 30$. It can be confirmed that the critical frequency is independent of k_2. Interestingly, the change of the critical frequency is proportional to that of the damping ratio. For typical values of soil damping, the frequency beyond which the extra visco-elastic surface wave exists may range from approximately 10 to 1000 Hz, as shown in Table 1. The extra surface wave therefore may be also of practical relevance, since this frequency range overlaps the typical frequency interval in which ground-borne vibration (1–80 Hz) and ground-borne noise (16–250 Hz) are of importance.

5.1. Determination of critical frequencies governing the number of surface wave

It is always possible to determine the critical frequencies by examining the positions of the discontinuities of the equivalent stiffness calculated including one pole (the quasi-elastic wave). Hereafter a systematic way is presented of the determination of the critical frequencies and therefore the frequency range in which two waves exist. First, the roots of Eq. (13) are analysed. Since the critical frequency is independent of k_2, hereafter $k_2 = 0.1$ is chosen for the following calculations and the parameters of the half-space are given by Eq. (33). To solve for the roots of Eq. (13), normally $\Delta = 0$ is rewritten to

$$\left(2\left(k_1^2 + k_2^2\right) - \omega^2 / \tilde{c}_{\mathrm{T}}^2\right)^2 = 4\tilde{R}_{\mathrm{L}}\tilde{R}_{\mathrm{T}}\left(k_1^2 + k_2^2\right) \tag{35}$$

and rationalized into a cubic equation with respect to k_1^2 by squaring both the left and right sides of Eq. (35). Using the Cardano's formula, three roots are obtained for k_1^2 of Eq. (35). Taking the square root of k_1^2, at least two roots are found in the first quadrant of the complex k_1 plane. It needs to be examined which ones of those are the admissible roots which satisfy the traction-free boundary condition and the radiation condition altogether.

From Fig. 6(b) it is known that $\omega_1 = 12.07$ Hz and $\omega_2 = 517.80$ Hz. In Fig. 7 the branch cuts, the branch points and the roots of the secular equation $\Delta = 0$ derived using the Cardano's formula in the first quadrant of the complex k_1 plane are plotted for a frequency $\omega < \omega_1 = 12.07$ (the $\omega < \omega_1$ surface) and another frequency $\omega_1 = 12.07 < \omega < \omega_2 = 517.80$ (the $\omega_1 < \omega < \omega_2$ surface). It can be seen that on the $\omega < \omega_1$ surface, there is only one pole representing the quasi-elastic wave. A spurious pole is located on the right-hand side of the branch cut for shear wave. However, on the surface on which $\omega_1 < \omega < \omega_2$, the pole of the quasi-elastic wave is still present, whereas the spurious pole crosses the branch cut for the shear wave and is now located in between the two branch cuts. The spurious pole becomes a pole for $\omega_1 < \omega < \omega_2$. To track this extra pole with increasing frequency, Fig. 8 shows the branch cuts, the branch points and the poles for a frequency on the $\omega_1 < \omega < \omega_2$ surface and a frequency on the $\omega_2 < \omega$ surface. Consistent with Fig. 6(a), a pole related to a visco-elastic surface wave exists in between the branch cuts for the P and S waves for $\omega_1 < \omega < \omega_2$. In contrast, when $\omega_2 < \omega$, the visco-elastic pole crosses the branch cut for the P wave and becomes a spurious pole again. Therefore, it can be assumed that the first critical frequency ω_1 is the frequency at which the pole for the visco-elastic wave is located on the branch cut for the S wave whereas the second critical frequency ω_2 is the one at which the pole for the visco-elastic wave is on the branch cut for the P wave. This observation is confirmed by investigating the branch line integrals S_{C2} and S_{C4} in Eq. (29). The branch integral S_{C2} at ω_1 has a discontinuity which indicates a pole on the path of integration C_2. Therefore, this pole and ω_1 satisfies

$$\begin{aligned} &\mathrm{Re}\left(\Delta\left(k_1 = k_1^{\mathrm{T}}\right)\right) = 0, \\ &\mathrm{Im}\left(\Delta\left(k_1 = k_1^{\mathrm{T}}\right)\right) = 0. \end{aligned} \tag{36}$$

After substituting Eqs. 22 and 23 into Eq. (36), ω_1 and the pole itself can be obtained for a specific value of k_2.

On the other hand, the extra pole may disappear after another frequency ω_2, and the critical point of disappearance is when the extra pole k_1^p is located on the branch C_4. Therefore, ω_2 and the pole satisfy

$$\begin{aligned} &\mathrm{Re}\left(\Delta\left(k_1 = k_1^{\mathrm{L}}\right)\right) = 0, \\ &\mathrm{Im}\left(\Delta\left(k_1 = k_1^{\mathrm{L}}\right)\right) = 0. \end{aligned} \tag{37}$$

Eqs. (36) and (37) together determine the frequency range in which two surface waves exist for visco-elastic half-space of the Kelvin-Voigt type.

5.2. Dependence of critical frequencies on Poisson's ratio and damping

It is of interest to investigate the dependence of the critical frequencies on the Poisson's ratio. A threshold of the Poisson's ratio $\nu^* = 0.2631$ is given in (O'Leary, 1981) and it is concluded that for all $\nu < \nu^*$ there is one and only one surface wave and for all $\nu > \nu^*$ there may be more than one surface wave for certain parameter combinations and frequency range. Therefore, critical frequencies, i.e. the boundaries which determine the number of poles (waves) are plotted versus the Poisson's ratio in Fig. 9 starting from $\nu = 0.27$. It can be concluded that the critical frequency is increasing with higher Poisson's ratio. In Fig. 9 (a) only ω_1 is plotted. The reason is that for relatively small viscosity, the second critical frequency ω_2 is large. For example, for $\nu = 0.27$, the second critical frequency ω_2 is about 5178 Hz. The second critical frequency ω_2 is even higher for $\nu > 0.27$ which is of no interest for train-induced ground vibration and furthermore the Euler-Bernoulli description of the rail is no longer valid for such high frequencies. In Fig. 9(b) both ω_1 and ω_2 are plotted for a higher damping ratio. It is found that both the two critical frequencies become larger for increasing Poisson's ratio. However, ω_2 increases much faster than ω_1. By comparing Fig. 9(a) and (b), it can be seen that larger damping ratio lowers the critical frequencies.

6. Conclusions

In this paper the equivalent stiffness of a visco-elastic half-space to a periodically supported beam under a moving load, as a model for train-track interaction, is investigated. A uniform expression is obtained for the entire velocity range of the moving load regardless of the ratio between the load speed and the wave speeds of the half-space. The equivalent stiffness is evaluated analytically by means of the contour integration method and residue theorem. It is found that, apart from the Rayleigh type surface wave, a second surface wave exists in a certain frequency range due to the viscosity of the half-space for typical parameters of the subsoil. The contribution of this second surface wave cannot be ignored. An effective method to determine the frequency range in which the visco-elastic wave exists is proposed. It is concluded that the critical frequencies for the occurrence of multiple surface waves are the ones at which a second pole of the integrand of the equivalent stiffness is located on one of the EJP branch cuts. The dependences of the related frequency range on the viscosity and Poisson's ratio are investigated. The critical frequencies increase with larger Possion's ratio whereas they decrease for highly viscous materials.

Declaration of competing interest

The authors declare that they have no known competing financial interests or personal relationships that could have appeared to influence the work reported in this paper.

Acknowledgements

This work has been made possible by funding from the Dutch rail infra provider ProRail in the domain of track condition monitoring. The first author would like to thank Dr. J.M. Barbosa from TU Delft for the discussion on the existence of a second root of the secular equation of a visco-elastic half-space.

References

Achenbach, J., 1975. Wave Propagation in Elastic Solids, vol. 16. Elsevier.
Carcione, J.M., 1992. Rayleigh waves in isotropic viscoelastic media. Geophys. J. Int. 108, 453–464. https://doi.org/10.1111/j.1365-246X.1992.tb04628.x.
Chen, Y., Wang, C., 2006. Steady-state response of a Timoshenko beam on an elastic half-space under a moving load. Acta Mech. Solida Sin. 19, 26–39. https://doi.org/10.1007/s10338-006-0604-x.
Chiriță, S., Ciarletta, M., Tibullo, V., 2014. Rayleigh surface waves on a Kelvin-Voigt viscoelastic half-space. J. Elasticity 115, 61–76. https://doi.org/10.1007/s10659-013-9447-0.
Currie, P., Hayes, M., O'Leary, P., 1977. Viscoelastic Rayleigh waves. Q. Appl. Math. 35, 35–53.
Currie, P., O'Leary, P., 1978. Viscoelastic Rayleigh waves II. Q. Appl. Math. 35, 445–454.
Degrande, G., Clouteau, D., Othman, R., Arnst, M., Chebli, H., Klein, R., Chatterjee, P., Janssens, B., 2006. A numerical model for ground-borne vibrations from underground railway traffic based on a periodic finite element–boundary element formulation. J. Sound Vib. 293, 645–666. https://doi.org/10.1016/j.jsv.2005.12.023.
Di, H., Zhou, S., Luo, Z., He, C., Xiao, J., Li, X., 2018. A vehicle-track-tunnel-soil model for evaluating the dynamic response of a double-line metro tunnel in a poroelastic half-space. Comput. Geotech. 101, 245–263. https://doi.org/10.1016/j.compgeo.2017.12.003.
Dieterman, H., Metrikine, A., 1996. The equivalent stiffness of a half-space interacting with a beam. critical velocities of a moving load along the beam. Eur. J. Mech. Solid. 15, 67–90.
Dieterman, H., Metrikine, A., 1997. Steady-state displacements of a beam on an elastic half-space due to a uniformly moving constant load. Eur. J. Mech. Solid. 16, 295–306.
Ewing, W., Jardetzky, W., Press, F., 1957. Elastic Waves in Layered Media. McGraw-Hill.
Forrest, J., Hunt, H., 2006. A three-dimensional tunnel model for calculation of train-induced ground vibration. J. Sound Vib. 294, 678–705. https://doi.org/10.1016/j.jsv.2005.12.032.
Galvín, P., François, S., Schevenels, M., Bongini, E., Degrande, G., Lombaert, G., 2010. A 2.5 D coupled FE-BE model for the prediction of railway induced vibrations. Soil Dynam. Earthq. Eng. 30, 1500–1512. https://doi.org/10.1016/j.soildyn.2010.07.001.
Hall, L., 2003. Simulations and analyses of train-induced ground vibrations in finite element models. Soil Dynam. Earthq. Eng. 23, 403–413. https://doi.org/10.1016/S0267-7261(02)00209-9.
Karlström, A., Boström, A., 2006. An analytical model for train-induced ground vibrations from railways. J. Sound Vib. 292, 221–241. https://doi.org/10.1016/j.jsv.2005.07.041.
Kononov, A., Wolfert, R.A., 2000. Load motion along a beam on a viscoelastic half-space. Eur. J. Mech. Solid. 19, 361–371. https://doi.org/10.1016/S0997-7538(99)00148-5.
Lamb, H., 1904. On the propagation of tremors over the surface of an elastic solid. Philos. Trans. R. Soc. London, Ser. A 203, 1–42. https://doi.org/10.1098/rsta.1904.0013.
Lombaert, G., Degrande, G., Francois, S., Thompson, D., 2015. Ground-borne Vibration Due to Railway Traffic: a Review of Excitation Mechanisms, Prediction Methods and Mitigation Measures. Springer, pp. 253–287. https://doi.org/10.1007/978-3-662-44832-8_33.
Metrikine, A., Popp, K., 1999. Vibration of a periodically supported beam on an elastic half-space. Eur. J. Mech. Solid. 18, 679–701. https://doi.org/10.1016/S0997-7538(99)00141-2.
Metrikine, A., Popp, K., 2000. Steady-state vibrations of an elastic beam on a visco-elastic layer under moving load. Arch. Appl. Mech. 70, 399–408. https://doi.org/10.1007/s004199900071.
Metrikine, A., Vrouwenvelder, A., 2000. Surface ground vibration due to a moving train in a tunnel: two-dimensional model. J. Sound Vib. 234, 43–66. https://doi.org/10.1006/jsvi.1999.2853.
O'Leary, P., 1981. Viscoelastic Rayleigh waves for constant Poisson's ratio. In: Proceedings of the Royal Irish Academy. Section A: Mathematical and Physical Sciences, 81A, pp. 147–155.
O'Leary, P., 1988. Surface vibration of a semi-infinite viscoelastic medium. In: Recent Developments in Surface Acoustic Waves. Springer, pp. 291–298.
O'Leary, P., 1989. Response of a class of low-loss viscoelastic materials to an oscillating source. In: Proceedings of the Royal Irish Academy. Section A: Mathematical and Physical Sciences, JSTOR, pp. 219–224.
Romeo, M., 2001. Rayleigh waves on a viscoelastic solid half-space. J. Acoust. Soc. Am. 110, 59–67. https://doi.org/10.1121/1.1378347.
Sharma, M., 2019. Rayleigh waves in isotropic viscoelastic solid half-space. J. Elasticity 1. https://doi.org/10.1007/s10659-019-09751-x.
Sheng, X., Jones, C., Petyt, M., 1999. Ground vibration generated by a load moving along a railway track. J. Sound Vib. 228, 129–156. https://doi.org/10.1006/jsvi.1999.2406.
Sheng, X., Jones, C., Thompson, D., 2006. Prediction of ground vibration from trains using the wavenumber finite and boundary element methods. J. Sound Vib. 293, 575–586. https://doi.org/10.1016/j.jsv.2005.08.040.
Shi, L., Selvadurai, A., 2016. Dynamic response of an infinite beam supported by a saturated poroelastic halfspace and subjected to a concentrated load moving at a constant velocity. Int. J. Solid Struct. 88, 35–55. https://doi.org/10.1016/j.ijsolstr.2016.03.027.
Steenbergen, M., Metrikine, A., 2007. The effect of the interface conditions on the dynamic response of a beam on a half-space to a moving load. Eur. J. Mech. Solid. 26, 33–54. https://doi.org/10.1016/j.euromechsol.2006.03.003.
Sun, H., Yang, Y., Shi, L., Geng, X., 2018. The equivalent stiffness of a saturated poroelastic halfspace interacting with an infinite beam under a moving point load. Soil Dynam. Earthq. Eng. 107, 83–95. https://doi.org/10.1016/j.soildyn.2018.01.022.
Triepaischajonsak, N., Thompson, D., 2015. A hybrid modelling approach for predicting ground vibration from trains. J. Sound Vib. 335, 147–173. https://doi.org/10.1016/j.jsv.2014.09.029.

Verruijt, A., Cońdova, C.C., 2001. Moving loads on an elastic half-plane with hysteretic damping. J. Appl. Mech. 68, 915–922. https://doi.org/10.1115/1.1410097.
Vostroukhov, A., 2002. Three-dimensional Dynamic Models of a Railway Track for High-Speed Trains (Ph.D. thesis).
Vostroukhov, A., Metrikine, A., 2003. Periodically supported beam on a visco-elastic layer as a model for dynamic analysis of a high-speed railway track. Int. J. Solid Struct. 40, 5723–5752. https://doi.org/10.1016/S0020-7683(03)00311-1.
Xia, Z., Wang, J., Xu, B., Lu, J., 2009. Equivalent stiffness of the saturated poro-elastic half space interacting with an infinite beam to harmonic moving loads. J. Shanghai Jiaot. Univ. 14, 385–392. https://doi.org/10.1007/s12204-009-0385-8.
Yang, Y.B., Hung, H.H., 2009. Wave propagation for train-induced vibrations: a finite/infinite element approach. World Sci. https://doi.org/10.1142/7062.
Ying, X., Katz, I.N., 1988. A reliable argument principle algorithm to find the number of zeros of an analytic function in a bounded domain. Numer. Math. 53, 143–163. https://doi.org/10.1007/BF01395882.
Yuan, Z., Xu, C., Cai, Y., Cao, Z., 2015. Dynamic response of a tunnel buried in a saturated poroelastic soil layer to a moving point load. Soil Dynam. Earthq. Eng. 77, 348–359. https://doi.org/10.1016/j.soildyn.2015.05.004.
Zhou, S., He, C., Guo, P., Di, H., Zhang, X., 2020. Modeling of vehicle-track-tunnel-soil system considering the dynamic interaction between twin tunnels in a poroelastic half-space. Int. J. GeoMech. 20, 04019144 https://doi.org/10.1061/(ASCE)GM.1943-5622.0001538.